

Imaging of Brain Tumor Proliferative Activity with Iodine-131-Iododeoxyuridine

Juri G. Tjuvajev, Homer A. Macapinlac, Farhad Daghighian, Andrew M. Scott, James Z. Ginos, Ronald D. Finn, Paresh Kothari, Revathi Desai, Jiaju Zhang, Bradley Beattie, Martin Graham, Steven M. Larson and Ronald G. Blasberg

Cotzias Neuro-Oncology Laboratory, Nuclear Medicine Service, Medical Physics Department, and Radiochemistry/Cyclotron Core Facility, Memorial Sloan-Kettering Cancer Center, New York, New York

Methods: Iodine-131-iododeoxyuridine (IUdR) uptake and retention was imaged with SPECT at 2 and 24 hr after administering a 10-mCi dose to six patients with primary brain tumors. The SPECT images were directly compared to gadolinium contrast-enhanced MR images as well as to [¹⁸F]fluorodeoxyglucose (FDG) PET scans and ²⁰¹Tl SPECT scans. **Results:** Localized uptake and retention of IUdR-derived radioactivity was observed in five of six patients. The plasma half-life of [¹³¹I]IUdR was short (1.6 min) in comparison to the half-life of total plasma radioactivity (6.4 hr). The pattern of [¹³¹I]IUdR-derived radioactivity was markedly different in the 2-hr compared to 24-hr images. Radioactivity was localized along the periphery of the tumor and extended beyond the margin of tumor identified by contrast enhancement on MRI. The estimated levels of tumor radioactivity at 24 hr, based on semiquantitative phantom studies, ranged between <0.1 and 0.2 μ Ci/cc (<0.001% and 0.002% dose/cc); brain levels were not measurable. **Conclusions:** Iodine-131-IUdR SPECT imaging of brain tumor proliferation has low (marginal) sensitivity due to low count rates and can detect only the most active regions of tumor growth. Imaging at 24 hr represents a washout strategy to reduce ¹³¹I-labeled metabolites contributing to background activity in the tumors, and is more likely to show the pattern of [¹³¹I]IUdR-DNA incorporation and thereby increase image specificity. Iodine-123-IUdR SPECT imaging at 12 hr and the use of [¹²⁴I]IUdR and PET will improve count acquisition and image quality.

Key Words: iododeoxyuridine; fluorodeoxyglucose; thallium-201-chloride; brain tumors; SPECT; PET

J Nucl Med 1994; 35:1407-1417

The biological and clinical manifestations of intracranial malignancy depend largely on the rate of tumor proliferation and increase in tumor size. Knowledge of tumor proliferative activity could be used to estimate tumor growth potential or grade of malignancy, and may be useful in

estimating the prognosis of patients with intracranial tumors. A noninvasive measurement of tumor cell proliferation could be helpful in the selection of optimal treatments and may provide an earlier measure of response to therapy when compared to tumor volume assessments by CT and MRI, or to measurements of tumor metabolism using 2-[¹⁸F]-fluoro-2-deoxy-D-glucose (FDG) and PET.

The use of halogenated pyrimidine nucleosides for studying the metabolic pathways of pyrimidine nucleoside incorporation into DNA and for measuring cell proliferation dates back more than 30 yr (1-5). Halogenated pyrimidine nucleosides have also been studied as potential chemotherapeutic agents (6-11), and have been used as radiation sensitizers (12-16) and as anti-viral agents (17-19). There are three major reasons for our interest in halogenated pyrimidines, particularly iododeoxyuridine (IUdR): (1) previous studies have demonstrated a substantial incorporation of radiolabeled IUdR into DNA of tumors and proliferating tissues (2,3,20-29); (2) low background radioactivity is achieved one or more days after intravenous administration due to rapid renal excretion of the major radiolabeled metabolite, iodide; and (3) the comparatively long physical half-lives of iodine radioisotopes ¹²⁴I (4.2 days), ¹³¹I (8.1 days) and ¹²³I (13 hr), are appropriate for longer IUdR studies. We (28,29) and others (30,31) have recognized that a time-dependent strategy for wash-out of radiolabeled metabolites over several hours (or days) can be used to reduce background radioactivity and increase the specificity of the resultant images with respect to IUdR-DNA incorporation.

In this pilot study we evaluated the potential utility of SPECT imaging of primary brain tumors at 2 and 24 hr after [¹³¹I]IUdR administration. We compared the location of [¹³¹I]IUdR uptake in the SPECT images with the regions of contrast enhancement on MRI. We also compared the [¹³¹I]IUdR images with ²⁰¹Tl uptake and [¹⁸F]FDG localization on corresponding SPECT and PET scans.

Received Jul. 28, 1993; revision accepted Mar. 28, 1994.

For correspondence or reprints contact: Ronald G. Blasberg, MD, Dept. of Neurology Rm. C799, Memorial Sloan Kettering Cancer Center, 1275 York Ave., New York, NY 10021.

METHODS

Patients

All patients were admitted to Memorial Sloan-Kettering Cancer Center with a diagnosis of primary tumors of the brain. Patients were >18 yr of age, had a Karnofsky score of ≥ 50 and had no known medical contraindications to MRI, CT, SPECT and PET scans. All patients had an initial MRI, and an [^{131}I]IUdR SPECT study; some patients also had ^{201}Tl SPECT and [^{18}F]FDG PET imaging of their tumors. All patients had tissue biopsies to confirm the type of tumor and establish the grade of malignancy.

Radiosynthesis and Purification of [^{131}I]IUdR

No-carrier-added ^{131}I -5-iodo-2-deoxyuridine ([^{131}I]IUdR) was prepared by reacting 2-deoxyuridine (UdR) with no-carrier added ^{131}I -labeled sodium iodide ([^{131}I]NaI) of high specific activity (8–12 Ci/mg) in an iodogen-coated reaction vial. Purification of the reaction solution was carried out by elution through Waters Sep Pak C18 cartridges with water followed by methanol. The [^{131}I]IUdR injection solution was prepared by evaporating the methanol-eluted fraction to dryness and dissolving the residue in a sterile physiological saline solution followed by terminal filtration for sterility. Radiochromatographic and ultraviolet analysis of the injection solution using HPLC showed a radiochemical purity of 99%–100% and the presence of trace amounts of UdR (9–24 μg). Radiochemical yield of [^{131}I]IUdR for five consecutive injectable preparations was $73.8\% \pm 8.3\%$. All preparations of [^{131}I]IUdR were proven to be sterile and apyrogenic.

Iodine-131-IUdR SPECT and Analysis of Images

All patients were pretreated with oral potassium iodide solution (10 drops SSKI TID) for 3 days prior to [^{131}I]IUdR administration in order to block thyroid uptake of radiolabeled iodide, the major radiolabeled metabolite of [^{131}I]IUdR. On the day of the study, patients received an intravenous injection of [^{131}I]IUdR (10 mCi) over 2 min and were imaged at 2 and 24 hr after [^{131}I]IUdR administration with a dual-headed ADAC Genesys gamma camera (Milpitas, CA) equipped with a lead collimator specially designed for high-resolution imaging of ^{131}I (hole diameter: 3.06, septa thickness 1.95, tunnel thickness 60 mm). All SPECT images of the brain were acquired in a 360° circular orbit, in a $64 \times 64 \times 16$ matrix with 64 stops at 60 sec per stop. Final images were processed with a Butterworth filter (0.3 cutoff, order 10), and the Chang attenuation correction was applied.

In order to obtain a rough estimate of [^{131}I]IUdR-derived radioactivity in the brain tumors of patients, two phantom studies were performed. In the first study, three plastic bags were filled with a 300-cc saline solution containing ^{131}I (0.1 $\mu\text{Ci}/\text{cc}$) to simulate background brain activity. The bags were placed inside a human skull to form a realistic phantom of the brain and two 12-cc plastic vials containing various concentrations of ^{131}I radioactivity were placed within this phantom. The phantom was imaged three times over a 2-wk interval, each time with a different concentration of radioactivity in the two vials ranging from 0.21 to 1.21 $\mu\text{Ci}/\text{cc}$. In the second phantom study, the skull was lined with a thin polyethylene film, filled with a freshly prepared 30% bisacrylamide solution containing 0.016 $\mu\text{Ci}/\text{cc}$ of [^{131}I]iodide to simulate brain background activity. Two 15-cc spherical "tumors" containing 0.23 and 0.33 $\mu\text{Ci}/\text{cc}$ were prepared from acrylamide gel, hardened, wrapped in polyethylene film and placed in the frontal and occipital pole of the liquid acrylamide "brain" prior to solidification. The phantom was imaged three times over a 2-wk interval; the radioactivity in the acrylic spheres ranged from 0.063

to 0.28 $\mu\text{Ci}/\text{cc}$ during imaging. The conditions of SPECT imaging, reconstruction and attenuation correction were the same as those described above for patient studies.

Regions of interest (ROIs) measurements (9 pixels, 3×3 square; $22 \text{ mm}^2/\text{pixel}$; the transaxial thickness of the slices was 2 pixels, 9.4 mm) were obtained in each of three or four contiguous slices. The mean counts/pixel values (\pm s.d.) were determined and plotted against the radioactivity concentration in each of the vials or acrylic spheres. The data from the two studies were comparable; they were combined and a linear fit of the data was performed. The resultant equation ($\mu\text{Ci}/\text{cc} = (0.0214 * \text{counts}/\text{pixel}) - 0.1584$) was used to estimate the ^{131}I radioactivity concentration in the SPECT images for those regions with ≥ 11 cts/pixel (corresponding to $\geq 0.08 \mu\text{Ci}/\text{cc}$; see Discussion and legends to Figs. 5 and 6). Patient tumors and normal brain were analyzed by drawing ROIs around the most active areas of tumor and within normal brain in contiguous slices, and a mean value was calculated.

Measurement of [^{131}I]IUdR and Radiolabeled Metabolites in Plasma

Serial arterial blood samples (2–3 ml) were obtained from a catheterized radial artery over 60 min after intravenous injection of [^{131}I]IUdR. Blood samples were stored on ice and then cold-centrifuged to obtain plasma. The radioactivity of plasma (nCi/ml) was measured by gamma spectroscopy and expressed as a percent of administered dose (% dose/ml plasma). One milliliter of plasma was treated with 5 ml of ice-cold 10% trichloroacetic acid (TCA) and cold-centrifuged at $12,000 \times g$ for 5 min. The acid-soluble fraction of plasma was removed, neutralized with NaOH and 0.5 ml was analyzed by HPLC. The HPLC system consisted of a HPXL Solvent Delivery System (Rainin Instrument Co. Inc.) and a Flo-One Beta detector Series 100 (Radiomatic) equipped with a gamma-cell detector (Radiomatic). Radiolabeled metabolite separation was accomplished with a 250×4.6 -mm, reverse-phase 10- μm C-18 column (Phenomenex); the isocratic mobile phase consisted of 15% methanol in water and the flow rate was 2 ml/min. Data were collected and analyzed using Dynamax[®] software (Rainin Instrument Co. Inc.). The integrated peaks of [^{131}I]IUdR, [^{131}I]iodouracil and [^{131}I]iodide were expressed as percent of total sample activity and used to calculate percent of administered dose per ml of plasma.

MRI

MRI studies were performed on a 1.5 Tesla GE Signa (General Electric Co., Milwaukee, WI) scanner. T2 (SE 2000/30,80) and T1 (500/20) weighted images with and without Gd-DTPA (0.22 cc/kg) were obtained in all patients within 2 wk of the SPECT and PET studies.

Thallium-201 SPECT

Thallium-201 was obtained commercially. SPECT images of the brain were obtained 20–30 min after intravenous injection of 4 mCi of ^{201}Tl with a dual-headed ADAC Genesys gamma camera (Milpitas, CA) equipped with a low-energy, high-resolution collimator. Acquisition parameters were 360° circular orbit, 64 stops at 60 sec per stop, with data acquired in $64 \times 64 \times 16$ matrix. Final images were processed with a Gaussian filter (0.2 cut off, order 20) and the Chang attenuation correction was applied. Tumor-to-brain uptake ratios were calculated from count data obtained within ROIs (as described above) drawn over the tumor area with the highest activity; and an area of the same size in the normal contralateral hemisphere (32).

Fluorine-18-FDG PET

Fluorine-18-2-fluoro-2-deoxy-D-glucose (USP) was produced by the cyclotron/chemistry core at MSKCC by the nucleophilic reaction utilizing the modifications recently described by Hamacher and Kothari (33,34). Patients were injected with 5–10 mCi of [¹⁸F]FDG and images of the brain were obtained 30 min after injection with a PC 4600 PET (Cyclotron Corp.) head camera (5 rings, 11-cm FOV). Data acquisition was performed over a 30-min period, 3 × 10-min frames, producing 27 contiguous interleaved axial slices 3.8 mm apart. The in-plane resolution of the scanner at the center is 11 × 10 mm FWHM. An analytic attenuation correction was applied to the final images and the data were expressed as nCi/g tissue. Tumor-to-brain uptake ratios were calculated from count data obtained from ROIs in the same slice by drawing an ROI around the tumor area with highest activity and a similar size region in normal white matter (35).

Image Registration

Thallium-201 SPECT, [¹⁸F]FDG PET and [¹³¹I]IUdR SPECT images were registered with corresponding Gd-DTPA-enhanced thallium-weighted MR images with software developed by Pelizzari et al. (36). Briefly, MR images on x-ray film were digitized with a video camera and transferred to a DEC Micro VAX II station (Maynard, CA). Surface contours of the brain were drawn on serial axial slices for matching FDG PET and MRI scans, and surface contours of the scalp were drawn on serial axial slices for matching SPECT and MRI studies. For 2-hr [¹³¹I]IUdR SPECT studies, the scalp was visible due to blood-pool activity, as well as sweat gland concentration and secretion of [¹³¹I]iodide. Therefore, the scalp was used as the surface contour for SPECT-MR image registration. The 24-hr [¹³¹I]IUdR SPECT images had low scalp activity compared to the 2-hr and thallium studies, and identification of the scalp contour was technically more difficult.

The three-dimensional surface contours of the SPECT and PET (“hat”) images were always fitted to the reference MR (“head”) images using a surface-matching algorithm that minimizes the mean square distance between points on the two surfaces. The SPECT and PET image data set was then resliced in the plane of the MR images. The two images (resliced SPECT and MRI, or resliced PET and MRI) were displayed adjacent to each other, and a “merged” or “combined” image was generated to facilitate anatomical localization of abnormal activity on the PET and SPECT images. Since the same MR image data set was used for registration of the IUdR, thallium and FDG images, direct comparisons between the resliced IUdR, thallium and FDG images could be made.

RESULTS

The results of our study are based on six patients with different brain tumors (Table 1). The age of the patients (5 males and 1 female) ranged from 27 to 59 yr. The six tumors included: two glioblastoma multiforme and one ependymoma, oligodendroglioma, anaplastic oligodendroglioma and gliosarcoma. The time between the onset of the disease symptoms and the imaging studies reported here ranged between 10 days and 5 yr. All patients were studied with Gd-DTPA-enhanced MRI and [¹³¹I]IUdR SPECT; five patients also had a ²⁰¹Tl SPECT study, and three out of this group had an [¹⁸F]FDG PET study.

TABLE 1

Estimate of Tumor and Brain [¹³¹I]IUdR-Derived Radioactivity

Patient	Age	Sex	Tumor	Estimated mean tissue activity*		
				Tumor		Brain
				2 hr	24 hr	2 hr
1	55	F	Glioblastoma multiforme	0.39	0.12	<0.1
2	27	M	Ependymoma	0.33	<0.1	<0.1
3	45	M	Anaplastic oligodendroglioma	0.69	0.10	<0.1
4	59	M	Gliosarcoma	0.44	0.19	<0.1
5	31	M	Oligodendroglioma	<0.1	—	<0.1
6	42	M	Glioblastoma multiforme	0.50 [†]	0.11 [‡]	<0.1 [†]

* μ Ci/cc, a rough estimate based on the results of phantom measurements (see Methods and Fig. 6).

[†]4-hr value.

[‡]18-hr value.

— indicates the study was not performed.

Uptake and Retention of [¹³¹I]IUdR

There were no complications or adverse reactions during or after intravenous administration of [¹³¹I]IUdR. Five of the six cases demonstrated significant uptake and retention of [¹³¹I]IUdR-derived radioactivity in the area of the brain tumor (Table 1). Tumor activity was highest during the earliest scan period (2 hr). There was no detectable [¹³¹I]IUdR uptake in one patient (Patient 5) with a low-grade oligodendroglioma. This lesion was visible only on T2-weighted MR images. There was no gadolinium contrast enhancement of the lesion on T1-weighted images indicating an intact blood-tumor barrier (BTB), and no uptake of ²⁰¹Tl was observed in this patient.

There were consistent differences in the pattern of radioactivity distribution at 2 and 24 hr after [¹³¹I]IUdR injection. Images obtained at 2 hr showed localization of radioactivity in areas that generally corresponded to the contrast-enhancing regions seen on MRI. Images obtained 24 hr after [¹³¹I]IUdR injection had considerably lower levels of radioactivity than the 2-hr images (Table 1). The areas of radioactivity were irregular in shape and were localized more along the periphery of the tumor and within the scalp or skull (Figs. 1E and 2E). In all cases, except Patient 5, the area of IUdR-derived radioactivity appeared to extend beyond the outer zone of contrast enhancement (Figs. 1E and 2E).

These findings are most clearly illustrated in a patient with glioblastoma multiforme (Patient 6) presented in Figure 3. The important issues illustrated by this patient are: (1) that [¹³¹I]IUdR-derived radioactivity appears to distribute to some regions of brain that do not contrast enhance (or have minimal and patchy contrast enhancement) on MR imaging; (2) that this pattern of distribution cannot be explained by misalignment during the registration of the SPECT and MR images; and (3) that radioactivity in these regions is retained for at least 24 hr. The extent of tumor infiltration suggested by the [¹³¹I]IUdR SPECT images was

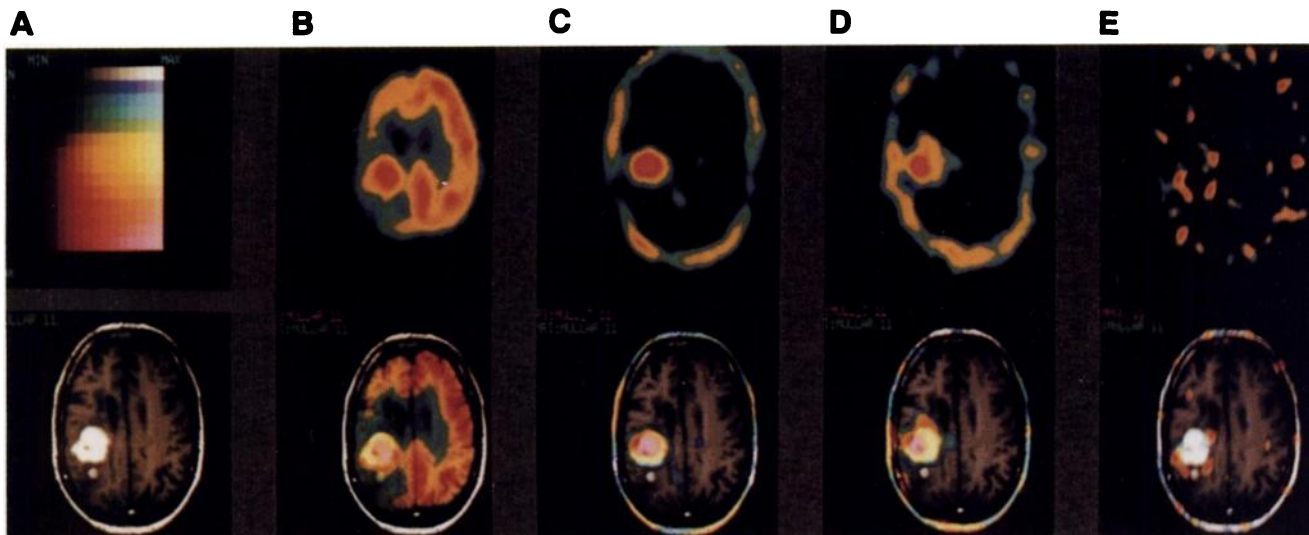


FIGURE 1. Comparison of contrast-enhanced MRI, $[^{18}\text{F}]\text{FDG}$ PET, ^{201}Tl SPECT and $[^{131}\text{I}]\text{IUdR}$ SPECT images and T1-weighted Gd-DTPA-enhanced MR, $[^{18}\text{F}]\text{FDG}$ PET, ^{201}Tl SPECT and $[^{131}\text{I}]\text{IUdR}$ SPECT images of Patient 4, a 59-yr-old male who had a right temporal lobe infarct in 1987 with persisting left hemiparesis. In 1991, the patient had a generalized convulsion and a MR scan showed a large enhancing right temporo-parietal lesion (A). The $[^{18}\text{F}]\text{FDG}$ PET scan indicated that the lesion was hypermetabolic and that the area of hypermetabolism was very similar to the areas of contrast enhancement and thallium uptake (B). The ^{201}Tl SPECT showed thallium uptake localized to the area of contrast enhancement (C). SPECT imaging performed at 2 hr after $[^{131}\text{I}]\text{IUdR}$ administration (D) showed a pattern of radioactivity distribution in the lesion that was similar, but not identical to the contrast-enhanced MR, thallium and FDG images; two foci of radioactivity appear to extend beyond the margin of contrast enhancement. Scalp activity at 2 hr reflects $[^{131}\text{I}]\text{I}$ in the blood pool, muscle and sweat glands. SPECT imaging repeated 24 hr after $[^{131}\text{I}]\text{IUdR}$ administration is "noisy" due to the low level of radioactivity (see Table 1). Three areas of retained radioactivity along the periphery of the lesion appear to extend beyond the border of contrast enhancement (E). This suggests that a high rate of tumor proliferation may be localized to the "infiltrating zone" of the tumor. The irregular pattern of scalp radioactivity at 24 hr probably reflects a combination of effects including nonuniform sweat gland concentration, secretion and accumulation of $[^{131}\text{I}]\text{I}$ salts on the surface of the skin, as well as nonuniform wiping of the scalp over the 24-hr period and the low counts in the image (low signal-to-noise ratio). Histological examination of the tumor revealed a gliosarcoma.

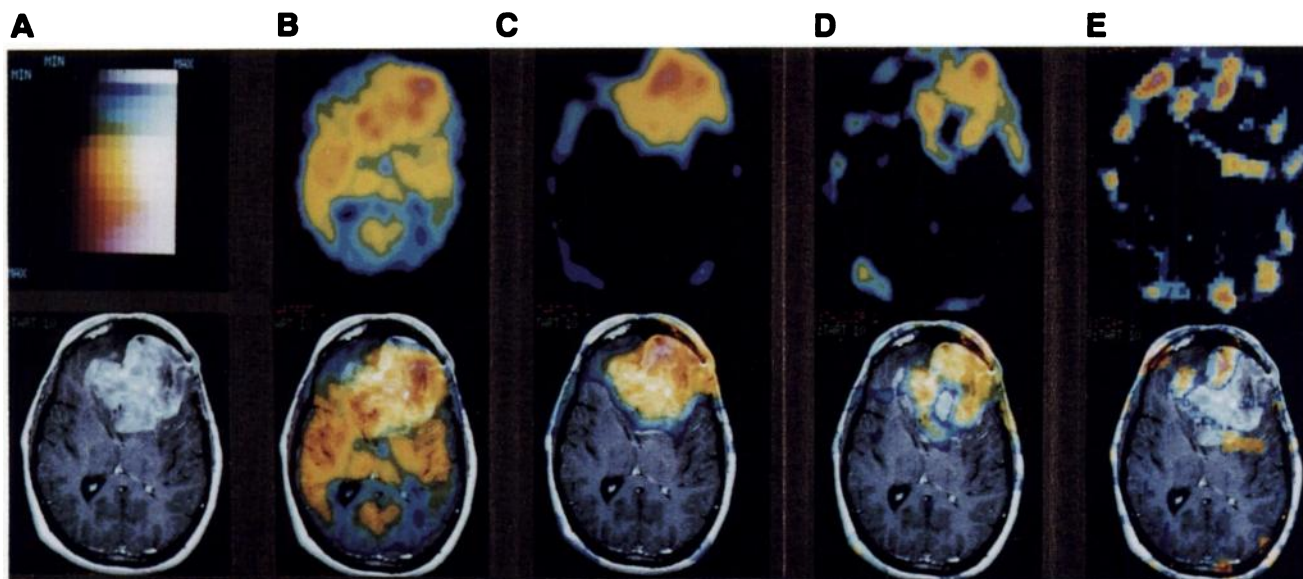


FIGURE 2. Comparison of contrast-enhanced MRI, $[^{18}\text{F}]\text{FDG}$ PET, ^{201}Tl SPECT and $[^{131}\text{I}]\text{IUdR}$ SPECT images and T1-weighted Gd-DTPA-enhanced MR, $[^{18}\text{F}]\text{FDG}$ PET, ^{201}Tl SPECT and $[^{131}\text{I}]\text{IUdR}$ SPECT images of Patient 3, a 45-yr-old male with an anaplastic oligodendroglioma (Patient 3) are shown prior to the second surgical procedure. The tumor at time of the initial resection was an oligodendroglioma which underwent malignant transformation during the 2-yr interval between surgical resections. The MR scan shows a large enhancing left frontal lesion extending beyond the midline into the right frontal lobe (A). Fluorine-18-FDG PET shows hypermetabolism (B) localized to the same distribution as contrast enhancement and thallium uptake. The ^{201}Tl SPECT scan shows uptake localized to the contrast-enhancing portions of the lesion (C). SPECT performed 2 hr after $[^{131}\text{I}]\text{IUdR}$ administration shows a heterogeneous pattern of $[^{131}\text{I}]\text{IUdR}$ -derived radioactivity activity distribution (D); note the low activity in the central zone of the tumor. Repeat imaging 24 hr after $[^{131}\text{I}]\text{IUdR}$ administration showed considerable washout of radioactivity from central tumor regions. The highest levels of $[^{131}\text{I}]\text{IUdR}$ -derived radioactivity are located around the periphery of the tumor and the scalp. This pattern of radioactivity distribution at 24 hr may reflect high proliferative activity in the infiltrating zone of this tumor as discussed in the legends to Figures 1 and 3.

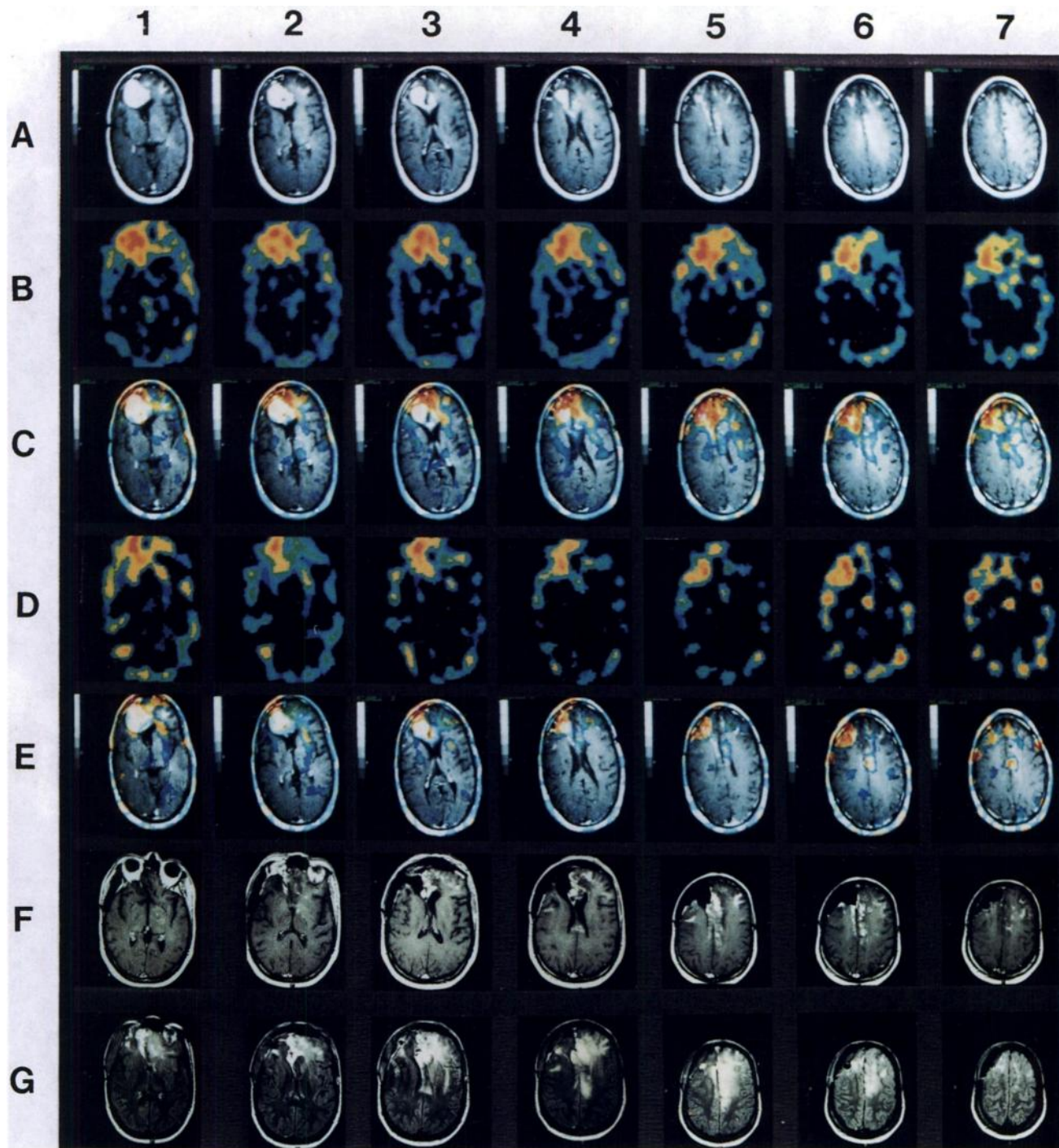


FIGURE 3. Comparison of MRI and ^{131}I IUdR SPECT imaging in Patient 6, a 42-yr-old male with a recurrent glioblastoma multiforme. The MR images (row A) show a large contrast-enhancing lesion in the right frontal lobe, involving the corpus callosum and extending across the midline into the left frontal lobe (A1–A4). There is also an extensive area of faint, patchy enhancement seen in the parasagittal subcortical white matter extending into the cortex which is more evident in the left hemisphere (A5–A7). The 2-hr ^{131}I IUdR SPECT images (row B) show that ^{131}I IUdR-derived radioactivity is largely localized to the contrast-enhancing portion of the tumor in the right hemisphere (C1–C4). Interestingly, high activity is also seen in the apical portion of the right frontal lobe where little or no contrast enhancement is seen (C5–C7). There are two areas of significant radioactivity in the superior left hemisphere: one localized to the frontal parasagittal area and extending apically into the subcortical white matter (C5–C7) which is barely contrast-enhancing on MRI (A5–A7); and there is another “sickle shaped” area extending around the frontal ventricle into the white matter lateral to the left caudate nucleus (C2–C5) which did not contrast enhance on MRI (A2–A5). SPECT images obtained 24 hr after ^{131}I IUdR injection (row D) revealed a retention of ^{131}I IUdR-derived radioactivity in the apical portion and the outer rim of the right frontal lesion (E1–E4). Substantial retention of radioactivity extended apically in the right frontal lobe (E5–E7) that was well beyond the patchy areas of minimal contrast enhancement observed on MRI (A5–A7). This observation suggests infiltrative tumor growth in this area. In the left hemisphere there was a substantial retention of radioactivity in the parasagittal subcortical white matter (E5–E7) and in the white matter lateral to the caudate nucleus (E1–E3), which also suggests infiltrative tumor growth. Although these selected regions did not show substantial contrast enhancement (A1–A7) or clearly abnormal proton density or T2 signal (images not shown) on MR at the time of the IUdR study, a follow-up MRI performed 1.5 mo later clearly shows contrast enhancement (row F) and an abnormal proton density signal (row G) in many of these areas as a result of tumor progression with BBB disruption. The imaging plane in the first study (rows A–E) is not identical to that in the second study (rows F–G).

TABLE 2
Tumor-Brain Activity Ratios of ^{18}F -Fluorodeoxyglucose and ^{201}Tl Uptake

Patient no.	Diagnosis	Localization	Activity ratio: Tumor-to-Brain	
			Thallium*	FDG†
1	Glioblastoma multiforme	Right temporal lobe	—	—
2	Ependymoma	III Ventricle	2.3	—
3	Anaplastic oligodendroglioma	Left frontal lobe	3-5	2.4
4	Gliosarcoma	Right temporal lobe	9-15	2.7
5	Oligodendroglioma	Right temporal lobe	1.0	—
6	Glioblastoma multiforme	Left temporal lobe	6.0	2.5

*Tumor-to-normal brain ratios.
†Tumor-to-normal white matter activity ratios.
— indicates the study was not performed.

not apparent on the MR images obtained on the same day. However, follow-up MR imaging 1.5 mo after the IUdR study and subtotal surgical resection of the tumor (rows F and G in Fig. 3) clearly show the presence of tumor in all brain areas that retained ^{131}I IUdR-derived radioactivity at 24 hr and were not resected at surgery. The pattern of contrast enhancement and abnormal proton density seen in the follow-up MRI study suggests that infiltrative tumor without BBB disruption may have been present in these nonresected brain areas, 1.5 mo earlier at the time of the ^{131}I IUdR SPECT study.

Comparison of ^{131}I IUdR Images with ^{201}Tl and ^{18}F FDG

The pattern of ^{201}Tl localization was similar to the contrast enhancement seen on T1-weighted MR images. Tu-

mor-to-contralateral brain ratios ranged from 2.3 to 15 in four of five patients; Patient 5 showed no thallium uptake (Table 2). The highest levels of radioactivity in the ^{201}Tl images were usually located in the center of the tumor, and gradually decreased toward the tumor margins (Figs. 1C and 2C). A similar or heterogenous pattern of radioactivity distribution in tumor was observed in three patients who had a ^{18}F FDG PET study; central tumor regions had the highest levels of radioactivity in one study (Fig. 1B) and were heterogenous in another (Fig. 2B); the tumor-to-contralateral white matter ratios ranged between 2.4 and 2.7 (Table 1). Images obtained 2 hr after ^{131}I IUdR injection (Figs. 1D and 2D) showed a pattern of isotope localization that was generally similar to that observed with ^{201}Tl or ^{18}F FDG, although some exceptions were noted (Figs. 1 and 2). Images obtained 24 hr after ^{131}I IUdR injection (Figs. 1E and 2E) showed substantial differences; most of the ^{131}I IUdR-derived radioactivity was in the periphery of the tumor as defined by the ^{201}Tl and ^{18}F FDG images.

Plasma Concentration of ^{131}I IUdR and Radiolabeled Metabolites

The time course (0–60 min) of arterial plasma radioactivity was measured after intravenous ^{131}I IUdR administration in Patients 4, 5 and 6. The acid-soluble fraction of the plasma samples was analyzed by HPLC and revealed two radiolabeled metabolites: ^{131}I iodide and ^{131}I iodouracil (Fig. 4A). The peak plasma concentration of ^{131}I IUdR was 0.025 ± 0.0026 (s.d.) %dose/ml and plasma radioactivity over the first 4 min was predominantly due to ^{131}I IUdR. At approximately 4 min after injection, the concentrations of ^{131}I IUdR and ^{131}I iodide were approximately equal ($\sim 0.004\%$ dose/ml). Iodine-131-iodide was the major radiolabeled metabolite. After 10 min, radiola-

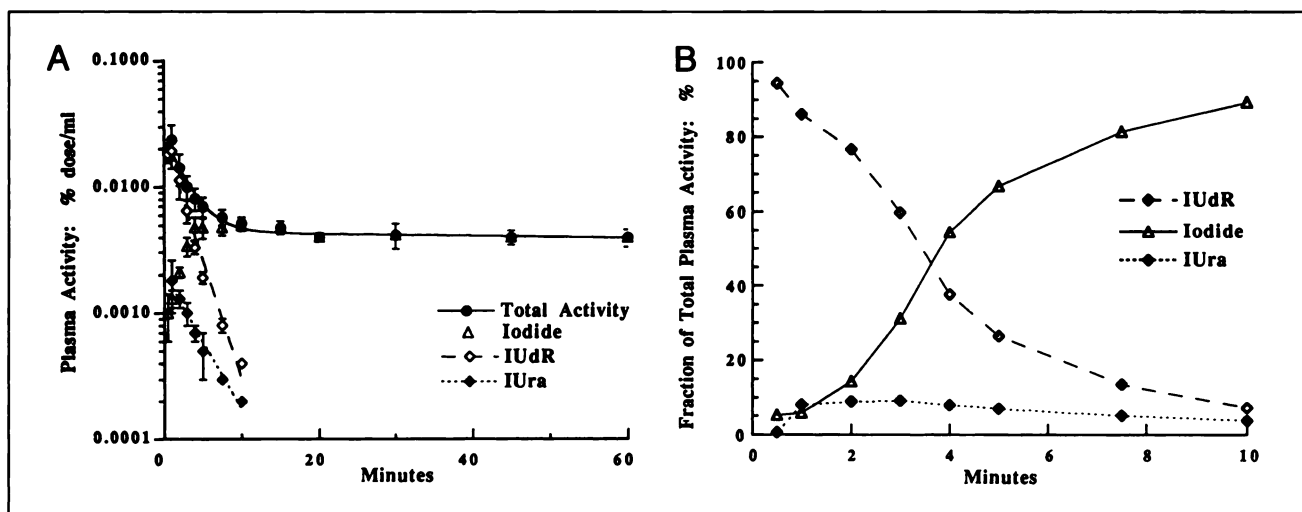


FIGURE 4. Plasma ^{131}I IUdR and radiolabeled metabolites. Mean values (\pm s.d.) of total plasma ^{131}I radioactivity and plasma concentrations of ^{131}I IUdR, ^{131}I iodouracil and ^{131}I iodide from three patients are plotted against time after intravenous injection of ^{131}I IUdR. Plasma concentration is expressed as %ID/ml of plasma (A) and as a fraction of total plasma radioactivity (B): ^{131}I IUdR (open diamonds), ^{131}I iodouracil (closed diamonds), ^{131}I iodide (open triangles), total plasma ^{131}I radioactivity (closed circles). The curve representing total plasma radioactivity can be described by the sum of two exponentials; the coefficients of the fit were $0.022\% \pm 0.003\%$ dose/ml and $-0.39 \pm 0.11 \text{ min}^{-1}$ for the first exponential, and $0.0044\% \pm 0.0017\%$ dose/ml and $-0.0018 \pm 0.011 \text{ min}^{-1}$ for the second exponential.

beled iodide accounted for >90% of total plasma radioactivity. Plasma [¹³¹I]iodouracil (IUra) was a minor radiolabeled metabolite. Iodine-131-IUra reached a peak value of 0.0018% ± 0.0008% dose/ml at 1 min and was always <10% of plasma total radioactivity (Fig. 4B). Plasma radioactivity after 10 min was essentially all due to [¹³¹I]iodide; values at 30 and 60 min were 0.0042% ± 0.0005% and 0.0039% ± 0.0006% dose/ml, respectively. The concentration time curve for total plasma radioactivity over the first 60 min could be adequately described by two exponentials (see legend to Fig. 4); the first exponential accounts for >80% of total radioactivity. The mean plasma half-lives of [¹³¹I]IUdR and [¹³¹I]IUra were estimated as 1.6 and 2.8 min, respectively.

DISCUSSION

Noninvasive imaging and measurements of tumor cell proliferation could aid in assessing grade of malignancy, contribute to treatment planning, and could provide an early assessment of treatment response prior to a change in tumor volume or glucose metabolism. The first in vivo studies of halogenated pyrimidine uptake and retention by tumors were performed in the late 1950s (1–5). More recently, 26 patients with tumors of different origin and body location were studied with planar imaging at 24 and 48 hr after the administration of 5–15 mCi of [¹³¹I]IUdR (31). In 50% of the patients there was evidence of [¹³¹I]IUdR-derived radioactivity localization in at least one tumor site. In three of four brain tumors, [¹³¹I]IUdR-derived radioactivity localized to the region of the tumor and high tumor-to-brain contrast was observed. These results were interpreted as showing [¹³¹I]IUdR incorporation into tumor DNA and the “stability” of [¹³¹I]IUdR-DNA incorporation over a 48-hr period (31).

Pharmacological Considerations of IUdR as an Imaging Tracer

IUdR is an analog of thymidine and is incorporated into nuclear DNA during the S-phase of cell division. The magnitude of radiolabeled IUdR incorporation into DNA is less than that of radiolabeled thymidine. The thymidine-to-IUdR incorporation ratio can vary in different tissues and is dependent on the site of radiolabeling of the precursor molecules (37); this is largely due to differences in metabolism and fate of the radiolabeled metabolites of thymidine and IUdR. IUdR incorporated into DNA is chemically stable over several days (20,29,38–40). Reutilization of IUdR during normal cell turnover is <10% (41) and there is only a small probability for IUdR reutilization at the polynucleotide and nucleotide levels in tumor cells (42). Thymidine reutilization has been shown to be about 46% greater than IUdR (55). The clearance half-time of DNA-incorporated IUdR from tumor tissue is in the order of 1–3 days and depends upon the rate of cell death and/or DNA repair (23). A major advantage of IUdR over other pyrimidine nucleosides is the availability of several isotopes of iodine to radiolabel IUdR with relatively long physical

half-lives. The iodine radionuclides that are suitable for imaging include ¹²³I ($t_{1/2} = 13$ hr) and ¹³¹I ($t_{1/2} = 8$ days) for SPECT and ¹²⁴I ($t_{1/2} = 4$ days) for PET.

These pharmacologic considerations and the availability of iodine radionuclides for SPECT and PET imaging led us to adopt a “washout strategy” to facilitate imaging IUdR-DNA incorporation 24 hr after IUdR administration when tissue background radioactivity was low (29). Rapid metabolic degradation of [¹³¹I]IUdR after systemic administration limits the fraction of administered dose incorporated into the DNA of dividing cells and the dominant radiolabeled metabolite, [¹³¹I]iodide, presents confounding problems for interpreting [¹³¹I]IUdR SPECT images during the first several hours after [¹³¹I]IUdR administration. We have shown in animal experiments that high levels of radiolabeled iodide are initially present in both plasma and tissue (29). The fraction of tumor radioactivity that was incorporated into DNA 1 hr after [¹³¹I]IUdR administration was small, ≤10% of total radioactivity; ≥90% tumor radioactivity was [¹³¹I]iodide at 1 hr.

Iodine-131-IUdR Imaging of the Brain Tumors

The first attempts to image brain tumors with radiolabeled halogenated pyrimidines were performed in the early 1960s (43) and 1970s (30). In this pilot investigation we begin to address the range of [¹³¹I]IUdR activities that can be imaged with SPECT. The results demonstrate the feasibility and limits of [¹³¹I]IUdR SPECT imaging of proliferative brain tumor activity. One important issue to address is the difference in the pattern of radioactivity distribution in the 2-hr and 24-hr images. The pattern of radioactivity observed at 2 hr generally resembled the pattern of blood-brain barrier (BBB) disruption observed in the contrast-enhanced MR images. This similarity is due to the rapid systemic metabolism of IUdR. Iodine-131-iodide accounts for all of plasma radioactivity at 30 and 60 min after [¹³¹I]IUdR administration. Thus, [¹³¹I]-IUdR-derived radioactivity imaged at 2 hr is likely to include a large fraction of [¹³¹I]iodide which crossed an altered BBB and could result in high [¹³¹I]iodide background activity within the tumor. At 24 hr, following substantial washout and total body clearance of the major radiolabeled metabolite ([¹³¹I]iodide), the pattern of [¹³¹I]IUdR-DNA incorporation in the tumor is more likely to be revealed in the SPECT image. We have shown a similar distribution pattern and washout of [¹³¹I]IUdR-derived radioactivity in rats with intracranial C6 gliomas (29,44). After 24 hr, >93% of measured tumor radioactivity was incorporated into tumor DNA in these animals.

The disparity between the 24-hr [¹³¹I]IUdR images and the [¹⁸F]FDG, ²⁰¹Tl and MR images can be explained by differences in metabolic pathways. The accumulation of [¹⁸F]FDG reflects glucose metabolism as well as the “lumped constant” in viable portions of the tumor (45,46). FDG accumulation and phosphorylation does not appear to be strongly related to proliferative activity of the tumors in vivo (47,48), or in vitro as measured by DNA flow

cytometry and ^3H -thymidine uptake (49). It has also been reported that glucose utilization does not vary significantly during different phases of the cell cycle (49). Thallium-201-chloride is a potassium-like analog which does not cross the normal BBB rapidly. In this respect, thallium imaging is similar to imaging contrast enhancement with MRI or CT. In addition to imaging the breakdown of the BBB of brain tumors, ^{201}Tl uptake is related to ATP-ase activity of the sodium-potassium pump and to active transmembrane transport in viable tumor cells (50,51). This results in a substantially greater accumulation of ^{201}Tl in viable (versus nonviable) portions of the tumor with a disrupted BBB. Thus, ^{201}Tl and ^{18}F FDG uptake primarily reflect viable and metabolically active, but not necessarily highly proliferative areas of the tumor.

The proliferative activity of tumor cells is known to be heterogeneous in larger tumors. We have recently shown a strong correlation between the level of ^{131}I IUdR incorporated into DNA in different tumor regions and corresponding measurements of labeling index and potential doubling time in rats with intracranial C6 gliomas using autoradiographic and immunohistochemical techniques (44). There was low or no proliferation and no ^{131}I IUdR-DNA incorporation in the central zone of many tumors, and high proliferation with high ^{131}I IUdR-DNA incorporation in the peripheral and infiltrative zone of tumor growth. The zones of ^{131}I IUdR-derived radioactivity in the SPECT images at 24 hr after ^{131}I IUdR administration are likely to represent regions of tumor with the highest proliferative activity and ^{131}I IUdR incorporated in tumor DNA. In all five of the patients with contrast-enhancing tumors, ^{131}I IUdR-derived radioactivity extended beyond the boundary of contrast enhancement and could represent the infiltrating zone of the tumor. These findings are supported by the well known fact that tumor progression, as well as tumor recurrences tend to occur in close proximity to the original contrast-enhancing margin of the tumor observed on CT or MR images. However, these observations must be tempered by the possibility of imprecise SPECT-MR image registration, partial volume effects and reconstruction artifacts resulting from low activity and noisy image data. Nevertheless, it is tempting to suggest that IUdR imaging has the potential for identifying the most active sites of tumor proliferation which has important implications for directing diagnostic stereotactic biopsies, for radiotherapy treatment planning, choosing the type of adjuvant therapy or defining the extent of surgical excision in each patient.

Pyrimidine nucleosides, including IUdR, do not cross normal brain capillaries rapidly (52). A facilitated transport system of low specificity for nucleosides is located at the blood-CSF barrier (the choroid plexus) (53,54), although choroid plexus uptake was not observed in the 2-hr SPECT images. Nucleosides have also been shown to diffuse across the ependyma, from CSF into parenchymal extracellular space, enter brain cells by facilitated transport and become phosphorylated (55). An intact BBB and the short

plasma half-life of IUdR will limit the amount of plasma IUdR that is delivered to brain and tumor cells. The presence of an intact BBB and the near absence of proliferative activity of normal brain tissue establishes an ideal background for imaging the proliferative activity of malignant brain tumors. Conversely, the presence of a blood-tumor barrier (BTB) would also limit the amount of IUdR delivered to tumor cells unless there is substantial facilitated transport of IUdR across tumor capillaries. This focuses on a potential limitation of using IUdR to image brain tumor proliferation. When blood-to-tumor transfer is limiting due to the BTB or to low blood flow, the amount of radiolabeled IUdR incorporated in tumor DNA could reflect the processes of delivery as well as tumor cell proliferation. This condition would adversely affect the clinical utility of the IUdR image data and establishes the necessity of documenting a contrast-enhancing tumor prior to performing IUdR studies in patients with brain tumors.

Patient 5 with a noncontrast-enhancing low-grade oligodendroglioma illustrates this point (Table 1). On the other hand, Patient 6 (Fig. 3) provides suggestive evidence for enhanced IUdR transport across capillaries supporting rapid growth of infiltrating tumor. This occurred in brain regions that did not contrast enhance on an MR scan that was obtained on the same day as the IUdR study. The presence of tumor in these regions was confirmed 1.5 mo later on a repeat MR scan. There are at least two possible explanations for these observations. One explanation is that passive BTB permeability is greater for nucleosides than for the larger gadolinium-DTPA molecule, and the other is that infiltrative gliomas may induce angiogenic factors which increase facilitated carrier-mediated transport of nucleosides.

Washout Strategy

Iodine-131-IUdR undergoes rapid metabolism after systemic administration, and iodide is the major radiolabeled metabolite. Greater than 80% of the administered dose is metabolized during the first 20 min after intravenous administration (3,20,22,29). There is a transient appearance of radiolabeled iodouracil (<10% total radioactivity) during the first 20 min following IUdR administration. Incorporation of ^{131}I IUra and ^{131}I iodide metabolites into DNA is insignificant (25,56). Plasma half-lives of ^{131}I IUdR and ^{131}I IUra in our study (1.6 and 2.8 min, respectively) were shorter than that described earlier (8,20,22,25,29,57). Radiolabeled iodide is cleared rapidly by the kidney; more than 70% is excreted in the urine during the first 24 hr (3,8,29,58,59). Thus, background radioactivity will be substantially lower 24 hr after IUdR administration compared to that at 1 or 2 hr. In support of a washout strategy, we have shown in animal experiments that >93% of total radioactivity measured in C6 gliomas is incorporated into DNA 24 hr after ^{131}I IUdR administration (29).

A similar washout strategy is not possible with ^{11}C -thymidine (TdR) imaging of tumor-proliferative activity. Measurements of ^{11}C radioactivity in tumor and normal

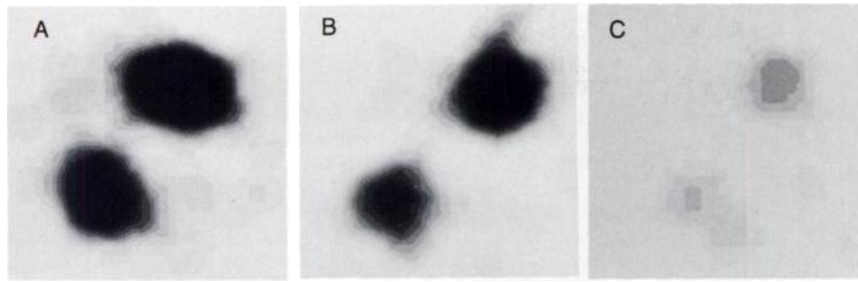


FIGURE 5. Low activity phantom images. Two 15-cc acrylic spheres were placed in a human skull and imaged at three different times (see Methods). Radioactivity levels at the time of imaging were: (A) 0.141 and 0.097 $\mu\text{Ci/cc}$; (B) 0.109 and 0.075 $\mu\text{Ci/cc}$; (C) 0.046 and 0.032 $\mu\text{Ci/cc}$, respectively. The same grey scale setting was used for all three sets of images.

tissues within 1 hr of methyl- ^{11}C -TdR administration include a large fraction of radiolabeled metabolites (60). The 20-min physical half-life of ^{11}C is too short to allow for sufficient tissue washout and body clearance of these metabolites. Recently it has been suggested that ^{11}C -labeling of TdR on the 2' position of the pyrimidine ring results in fewer radiolabeled metabolites and that an increased percent of total tissue radioactivity is measured in the acid-insoluble or DNA fraction at 1 hr following 2'- ^{11}C -TdR (80%) compared to a methyl- ^{11}C -TdR (40%) injection (61,62). However, substantially greater amounts of ^{11}C -labeled carbon dioxide and bicarbonate are measured following administration of 2'- ^{11}C -TdR. It has been shown in the dog that the predominant fraction of blood radioactivity is ^{11}C - CO_2 / ^{11}C - CO_3^- 3 min after 2'- ^{11}C -TdR administration; ^{11}C - CO_2 / ^{11}C - CO_3^- accounts for approximately 70% of total blood activity between 5 and 60 min and only 47% of total administered radioactivity is exhaled over 10 min (63). At least 25% of blood radioactivity will be reflected in background tissue radioactivity due to bicarbonate (64).

A similar limitation exists with previous attempts to measure the uptake and retention of ^{18}F -labeled pyrimidines (5-fluorouracil, 5-fluorouridine and 5-fluorodeoxyuridine) in tumors with PET. Fluorine-18-labeled 5'-fluoropyrimidines were synthesized, administered intravenously, and radioactivity in the tumor was measured or visualized in several studies (65–68). Insufficient washout of ^{18}F -labeled metabolites in tumor and surrounding tissues contributed to high background radioactivity during the period of imaging or tissue sampling. Fluorine-18-fluoride liberated by dehalogenation is avidly accumulated by bone despite the fairly rapid excretion of fluoride by the kidney. Fluorine-18-labeled 5'-fluoropyrimidines are also incorporated into the RNA of nondividing cells which limits the specificity of the assessment. A washout strategy could not be used in these studies because of the short 110-min physical half-life of ^{18}F , and this limits the usefulness of the ^{18}F -labeled pyrimidines for metabolic imaging.

Limits of ^{131}I UdR SPECT Imaging

A major limitation of this pilot study was the low level of radioactivity in the tumors. In an attempt to evaluate the reliability of the noisy patient images, particularly the peripheral localization of radioactivity in the tumors at 24 hr (Figs. 1–3), and to obtain a rough estimate of radioactivity in the tumors (Table 1), two phantom studies were per-

formed (see Methods). Images of two 15-cc spheres containing different levels of radioactivity that were placed within a human skull were obtained (Fig. 5); the same camera, acquisition, reconstruction and attenuation parameters were used as in the patient studies. A reasonable spherical image is obtained at 0.141 and 0.096 $\mu\text{Ci/cc}$, whereas at lower levels of radioactivity, the sphere and its margins were less well defined. The image was degraded at the lowest activity (0.032 $\mu\text{Ci/cc}$), but peripheral or ring enhancement around the sphere was not observed. Thus, IUDR imaging has the potential for identifying the most active sites of brain tumor proliferation and radioactivity that localized along the periphery of the tumors is not likely to be an artifact of the reconstruction process.

Rough quantitation based on a calibration curve generated from the phantom studies (Fig. 6) suggests that mean levels of tumor radioactivity ranged between <0.1 to 0.69 $\mu\text{Ci/cc}$ at 2 hr (<0.001% to 0.0069% dose/g, respectively) (Table 1). However, the early SPECT images are likely to include a large fraction of ^{131}I iodide as discussed above. The 24-hr images, following washout of nonincorporated radioactivity, were noisy and of poor quality due to low counts; the mean levels of retained radioactivity in tumor were estimated to range between <0.1 and 0.19 $\mu\text{Ci/cc}$

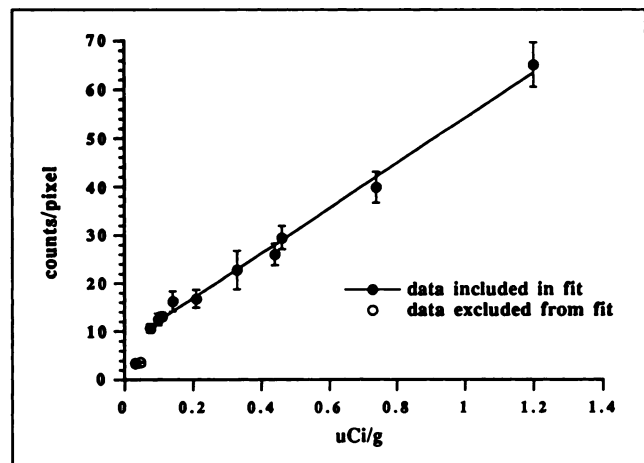


FIGURE 6. Phantom calibration. Two phantom studies were performed (see Methods) and the results were plotted: cts/pixel (ordinate) versus $\mu\text{Ci/cc}$ (abscissa). A linear relationship was observed above 0.08 $\mu\text{Ci/cc}$, but the line did not extrapolate through zero. Below 0.08 $\mu\text{Ci/cc}$ the curve appeared to be nonlinear. We limited our rough estimates of tissue radioactivity to ROI measurements of ≥ 11 counts/pixel ($\sim \geq 0.08$ $\mu\text{Ci/cc}$).

(<0.001% to 0.0019% dose/g, respectively). Thus, SPECT imaging of human brain tumor proliferation with [¹³¹I]IUdR has low (marginal) sensitivity and can detect only the most active regions of tumor growth. The levels of [¹³¹I]IUdR-derived radioactivity are in the same range as calculated from our previous animal experiments (29). Tumor radioactivity in C6 gliomas ranged between 0.01% to 0.4% dose/g tissue. Using these values and a 1/200 rat-to-human conversion factor (based on weight differences), a 10-mCi dose of IUdR administered to patients would be expected to result in tumor activities between 0.005 and 0.20 μ Ci/cc tissue.

Based on the results of this study, it is likely that more successful imaging of IUdR incorporation into tumor DNA with SPECT requires the use of a higher dose of [¹³¹I]IUdR, longer imaging times and multiheaded SPECT cameras in order to acquire a greater number of counts. The use of [¹²³I]IUdR and imaging at 12 hr after administration will increase counting efficiency several-fold due to the greater sensitivity of gamma cameras to lower energy ¹²³I emissions and will result in improved image quality. In addition, a higher dose of [¹²³I]IUdR can be administered due to dosimetry differences between ¹²³I and ¹³¹I radionuclides. The use of ¹²⁴I-labeled IUdR and PET will result in a further increase in sensitivity and image quality, particularly with the new "septa-out" tomographs. Good quantitation of ¹²⁴I radioactivity, despite the large number of non-511 keV gamma emissions, using different PET tomographs has been shown by us and others (69–74).

ACKNOWLEDGMENT

This study was supported in part by Department of Energy grant DE-FG02-86ER 60407.

REFERENCES

- Eidinoff M, Cheong L, Rich M. Incorporation of unnatural pyrimidine bases into deoxyribonucleic acid of mammalian cells. *Science* 1959;129:1550–1551.
- Prusoff W. Incorporation of iododeoxyuridine, an analog of thymidine, into mammalian deoxyribonucleic acid. *Fed Proc* 1959;18:305.
- Prusoff W, Jaffe J, Gunther H. Studies in the mouse of the pharmacology of 5-iododeoxyuridine, an analogue of thymidine. *Biochem Pharmacol* 1960;3:110–121.
- Krueger R, Gittlin D, Commerford S, et al. Iododeoxyuridine as a tracer of DNA metabolism in vivo. *Fed Proc* 1960;19:307.
- Xeros N. Deoxyriboside control and synchronization of mitosis. *Nature* 1962;194:682–683.
- Mathias A, Fischer G, Prusoff W. Inhibition of the growth of mouse leukemia cells in culture by 5-iododeoxyuridine. *Biochim Biophys Acta* 1959;36:560–561.
- Eidinoff M, Cheong L, Gambetta G, et al. Incorporation of 5-iodouracil labeled with iodine-131 into the deoxyribonucleic acid of human leukaemic leucocytes following in vivo administration of 5-iododeoxyuridine labeled with iodine-131. *Nature* 1959;183:1686–1687.
- Calabresi P, Cardoso S, Finch S, et al. Initial clinical studies with 5-iodo-2'-deoxyuridine. *Cancer Res* 1961;21:550–559.
- Lee S, Giovannella B, Stehlin J. Effect of excess thymidine on the growth of human melanoma cells transplanted in thymus deficient nude mice. *Cancer Lett* 1977;3:209–214.
- Howell S, Chu B, Mendelsohn J, et al. Thymidine as a chemotherapeutic agent: pharmacologic, cytokinetic, and biochemical studies in a patient with T-cell acute lymphocytic leukemia. *J Natl Cancer Inst* 1980;65:277–284.
- Bruno S, Poster D, Bono V, et al. High-dose thymidine in clinical oncology. *Cancer Treat Rep* 1981;65:57–63.

- Djordjevic B, Szybalski W. Genetics of human cell lines III incorporation of 5-bromo and 5-iododeoxyuridine into the deoxyribonucleic acid of human cells and its effect on radiation sensitivity. *J Exp Med* 1960;112:509–531.
- Kinsella T, Collins J, Rowland J, et al. Pharmacology and phase I/II study of continuous intravenous infusions of iododeoxyuridine and hyperfractionated radiotherapy in patients with glioblastoma multiforme. *J Clin Oncol* 1988;6:871–879.
- Greenberg H, Chandler W, Diaz R, et al. Intra-arterial bromodeoxyuridine radiosensitization and radiation in treatment of malignant astrocytomas. *J Neurosurg* 1988;69:500–505.
- Lawrence T, Davis M, Maybaum J, et al. The dependence of halogenated pyrimidine incorporation and radiosensitization on the duration of drug exposure. *Int J Radiat Oncol Biol Phys* 1990;18:1393–1398.
- Sondak V, Lawrence T, Ensminger W, Chang A. Preoperative IUdR and radiation for soft tissue sarcomas: preliminary results and normal tissue IUdR-incorporation data. *Proc Ann Meet Am Soc Clin Oncol* 1990;9:A1228.
- Watanabe K, Reichman U, Hirota K, Lopez C, et al. Nucleosides 110 synthesis and antiherspes virus activity of some 2'-fluoro-2'-deoxyarabino-furanosylpyrimidine nucleosides. *J Med Chem* 1979;22:21–24.
- Watanabe K, Su T, Klein R, et al. Nucleosides 123 synthesis of antiviral nucleosides: 5-substituted 1-(2-deoxy-2-halogeno- β -D-arabinofuranosyl)cytosines and -uracils. Some structure-activity relationships. *J Med Chem* 1983;28:152–156.
- Price R, Cardle K, Watanabe K. The use of antiviral drugs to image herpes encephalitis. In: Lopez B, ed. *Human herpes virus infections*. New York: Raven Press; 1986:7–15.
- Hampton E, Eidinoff M. Administration of 5-iododeoxyuridine-1131 in the mouse and rat. *Cancer Res* 1961;21:345–352.
- Calabresi P, Finch S, Cardoso S, Welch A. Preliminary clinical experiences with 5-iododeoxyuridine. *Proc Am Assoc Cancer Res* 1960;3:99.
- Kriss J, Maruyama Y, Tung L, et al. The fate of 5-bromodeoxyuridine, 5-bromodeoxycytidine, and 5-iododeoxycytidine in Man. *Cancer Res* 1963;23:260–268.
- Hofer K, Prenskey W, Hughes W. Death and metastatic distribution of tumor cells in mice monitored with ¹²⁵I-iododeoxyuridine. *J Nat Cancer Inst* 1969;43:763–773.
- Dethlefsen L. Incorporation of iodine-125-labeled 5-iodo-2'-deoxyuridine into the DNA of mouse mammary tumors. In: Fry R, ed. *Normal and malignant cell growth*. New York: Springer-Verlag; 1969:186–201.
- Klecker R, Jenkins J, Kinsella T, et al. Clinical pharmacology of 5-iodo-2'-deoxyuridine and 5-iodouracil and endogenous pyrimidine modulation. *Clin Pharmacol Ther* 1985;38:45–51.
- Bagshawe K, Sharma S, Southall P, et al. Selective uptake of toxic nucleoside (¹²⁵IUdR) by resistant cancer. *Br J Radiol* 1991;64:37–44.
- Humm J, Bagshawe K, Sharma S, Boxer G. Tissue dose estimates following the selective uptake of ¹²⁵IUdR and other radiolabeled thymidine precursors in resistant tumors. *Br J Radiol* 1991;64:45–49.
- Tjuvajev J, Muraki A, Berke J, et al. Iododeoxyuridine (IUdR) uptake and retention as a measure of tumor growth. *Neurology* 1992;42:190–191.
- Tjuvajev J, Muraki A, Ginos J, et al. Iododeoxyuridine (IUdR) uptake and retention as a measure of tumor growth. *J Nucl Med* 1993;34:1152–1161.
- Schuhmacher J, Kampmann H, Mattern J, et al. Incorporation of ¹³¹I-iododeoxyuridine into DNA of tumor-bearing rats after partial synchronization as a tool in scintigraphic tumor localization. *Nucl Med* 1974;12:309–319.
- Philip P, Bagshawe K, Searle F, et al. In vivo uptake of ¹³¹I-5-iodo-2-deoxyuridine by malignant tumors in man. *Br J Cancer* 1991;63:134–135.
- Kim KT, Black KL, Mariano D, et al. Thallium-201 SPECT imaging of brain tumors: methods and results. *J Nucl Med* 1990;31:965–969.
- Hamacher K, Coenen HH, Stocklin G. Efficient stereospecific synthesis of no-carrier-added 2-¹⁸F-fluoro-2-deoxy-D-glucose using aminopolyether supported nucleophilic substitution. *J Nucl Med* 1986;27:235–238.
- Kothari P, Ginos J, Finn R, et al. *Cryptand* (2.2.2) quantitation in the synthesis of ¹⁸F-2-fluoro-2-deoxy-D-glucose. In: *Workshop on targeting and target chemistry*. Villigen, Switzerland: PSI; 1991:18–21.
- DiChiro G, DeLaPaz R, Brooks R, et al. Glucose utilization of cerebral gliomas measured by (¹⁸F) fluorodeoxyglucose and positron emission tomography. *Neurology* 1982;32:1323–1329.
- Pelizzari CA, Chen CT, Spelbring DR, Weichselbaum RR. Accurate three-dimensional registration of CT, PET, and/or MR images of the brain. *J Comput Assist Tomogr* 1989;13:20–26.
- Hopkins HA, Wakefield JA. Utilization of ³H from deoxyuridine and thymidine for synthesis of DNA and other macromolecules in various organs of the rat. *Biochem Pharmacol* 1977;26:59–64.

38. Dethlefsen L. Reutilization of ¹³¹I-5-iodo-2'-deoxyuridine as compared to ³H-thymidine in mouse duodenum and mammary tumor. *J Nat Cancer Inst* 1970;44:827-840.
39. Hume WJ, Saffhill R. Iodo- and bromodeoxyuridine are excised at different rates from DNA of mouse tongue keratinocytes in vitro. *Chem Biol Interact* 1986;60:227-232.
40. Quackenbush RC, Shields AF. Local re-utilization of thymidine in normal mouse tissues as measured with iododeoxyuridine. *Cell Tissue Kinetics* 1988;21:381-387.
41. Hughes WL, Commerford SL, Gitlin D, et al. Deoxyribonucleic acid metabolism in vivo. 1. Cell proliferation and death as measured by incorporation and elimination of iododeoxyuridine. *Federation Proc* 1965;23:640-648.
42. Lee D, Prenskey W, Krause G, Hughes W. Blood thymidine level and iododeoxyuridine incorporation and reutilization in DNA in mice given long-acting thymidine pellets. *Cancer Res* 1976;36:4577-4583.
43. Kriss J, Revesz L. The distribution and fate of bromodeoxyuridine and bromodeoxycytidine in the mouse and rat. *Cancer Res* 1962;22:254-265.
44. Tjuvajev J, Abrams D, Ginos J, et al. Iododeoxyuridine (IUdR) imaging of tumor proliferation: correlation with kinetic parameters of local tumor cell proliferation. *Neurology* 1993;43:A399.
45. Kapoor R, Spence A, Muzi M, et al. Determination of the deoxyglucose and glucose phosphorylation ratio and the lumped constant in rat brain and a transplantable rat glioma. *J Neurochem* 1989;53:37-44.
46. Spence A, Graham M, Muzi M, et al. Deoxyglucose lumped constant estimated in a transplanted rat astrocytic glioma by the hexose utilization index. *J Cereb Blood Flow Metab* 1990;10:190-198.
47. Minn H. Fluorodeoxyglucose imaging: a method to assess the proliferative activity of human cancer in vivo: comparison with DNA flow cytometry in head and neck tumors. *Cancer* 1988;61:1776-1781.
48. Haberkorn U, Strauss L, Reisser C, et al. Glucose uptake, perfusion and cell proliferation in head and neck tumors: relation of positron emission tomography to flow cytometry. *J Nucl Med* 1991;32:1548-1555.
49. Higashi K, Clavo A, Wahl R. Does FDG uptake measure proliferative activity of human cancer cells? In vitro comparison with DNA flow cytometry and tritiated thymidine uptake. *J Nucl Med* 1993;34:414-421.
50. Ando A, Ando I, Katayama M, et al. Biodistributions of radioactive alkaline metals in tumor bearing animals: comparison with ²⁰¹Rl. *Dur J Nucl Med* 1988;14:352-357.
51. Brismar T, Collins V, Kesselberg M. Thallium-201 uptake relates to membrane potential and potassium permeability in human glioma cells. *Brain Res* 1989;500:30-36.
52. Conford EM, Oldendorf WA. Independent blood-brain barrier transport systems for nucleic acid precursors. *Biochim Biophys Acta* 1975;394:211-219.
53. Spector R. Thymidine transport in the central nervous system. *J Neurochem* 1980;35:1092-1098.
54. Spector R. Thymidine accumulation by choroid plexus in vitro. *Arch Biochem Biophys* 1980;205:85-93.
55. Spector R, Berlinger W. Localization and mechanism of thymidine transport in the central nervous system. *J Neurochem* 1982;39:837-841.
56. Cooper V, Dunning W, Greer S. Role of catabolism in pyrimidine utilization and for nucleic acid synthesis in vivo. *Cancer Res* 1972;32:390-397.
57. Russo A, Gianni L, Kinsella T, et al. Pharmacological evaluation of intravenous delivery of 5-bromodeoxyuridine to patients with brain tumors. *Cancer Res* 1984;44:1702-1705.
58. Welch A, Jaffe J, Cardoso S, et al. Studies on the pharmacology of 5-iododeoxyuridine in animals and man. *Proc Am Assoc Cancer Res* 1960;3:161.
59. Welch A, Prusoff W. A synopsis of recent investigations of 5-iodo-2'-deoxyuridine. *Cancer Chemother Reports* 1960;6:29-36.
60. Shields AF, Lim K, Grierson J, et al. Utilization of labeled thymidine in DNA synthesis: studies for PET. *J Nucl Med* 1990;31:337-342.
61. Shields AF, Kozell LB, Link JM, et al. Comparison of PET imaging using (C-11)thymidine labeled in the ring-2 and methyl positions [Abstract]. *J Nucl Med* 1990;31:794.
62. Shields AF, Swenson ER, Bassingthwaite JB. Contribution of labeled carbon dioxide to PET imaging of ¹¹C-labeled compounds. *J Nucl Med* 1992;33:581-586.
63. Shields AF, Graham MM, Kozawa SM, et al. Contribution of labeled carbon dioxide to PET imaging of carbon-11-labeled compounds. *J Nucl Med* 1992;33:581-584.
64. Gjedde A. Labeled carbon dioxide: how transient a metabolite. *J Nucl Med* 1992;32:585-586.
65. Abe Y, Fukuda H, Ishiwata K, et al. Studies on ¹⁸F-labeled pyrimidines. Tumor uptakes of ¹⁸F-5-fluorouracil, ¹⁸F-5-fluorouridine, and ¹⁸F-5-fluorodeoxyuridine in animals. *Eur J Nucl Med* 1983;8:258-261.
66. Ishiwata K, Ido T, Kawashima K, Murakami M, et al. Studies on ¹⁸F-labeled pyrimidines. II. Metabolic investigation of ¹⁸F-5-fluorouracil, ¹⁸F-5-fluoro-2'-deoxyuridine and ¹⁸F-5-fluorouridine in rats. *Eur J Nucl Med* 1984;9:185-189.
67. Ishiwata K, Ido T, Abe Y, Matsuzawa T, et al. Studies on ¹⁸F-labeled pyrimidines III. Biochemical investigation of ¹⁸F-labeled pyrimidines and comparison with 3H-deoxythymidine in tumor-bearing rats and mice. *Eur J Nucl Med* 1985;10:39-44.
68. Tsurumi Y, Kameyama M, Ishiwata K, et al. Fluorine-18-fluoro-2'-deoxyuridine as a tracer of nucleic acid metabolism in brain tumors. *J Neurosurg* 1990;72:110-113.
69. Miraldi F. Monoclonal antibodies and neuroblastoma. *Semin Nucl Med* 1989;19:282-294.
70. Kairemo K, Daghighian F, Brownell A, et al. Positron emission tomography (PET) for diagnosis of ovarian cancer metastases using I-124-labeled monoclonal antibody in a nude rat model [Abstract]. *J Nucl Med* 1990;31:764.
71. Bakir M, Babich J, Styles J, et al. Iodine-124-labeled-ICR12, a new monoclonal antibody for imaging proto-oncogene expression in breast cancer using PET: optimization of labeling efficiency and immunoreactivity [Abstract]. *J Nucl Med* 1990;31:777.
72. Pentlow K, Graham M, Daghighian F, et al. The use of positron emission tomography for quantitative imaging of I-124 labeled antibodies [Abstract]. *J Nucl Med* 1990;31:864.
73. Langen K, Coenen H, Roosen N, et al. SPECT studies of brain tumors with L-3-(123I) iodo- α -methyl tyrosine: comparison with PET, ¹²⁴IMT and first clinical results. *J Nucl Med* 1990;31:281-286.
74. Pentlow KS, Graham MC, Lambrecht RM, Cheung N-KV, Larson SM. Quantitative imaging of I-124 using positron emission tomography with applications to radioimmunodiagnosis and radioimmunotherapy. *Med Phys* 1991;18:357-366.